Transp Porous Med (2012) 95:425–446
DOI 10.1007/s11242-012-0053-6

Absolute/Convective Instability Dichotomy in a Soret-Driven Thermosolutal Convection Induced in a Porous Layer by Inclined Thermal and Vertical Solutal Gradients

Leonid Brevdo · Olaf A. Cirpka

Received: 5 April 2012 / Accepted: 21 July 2012 / Published online: 7 August 2012

Abstract In this article, we extend the analysis of Diaz and Brevdo (J. Fluid Mech. 681:567–596, 2011) of the absolute/convective instability dichotomy at the onset of convection in a saturated porous layer with either horizontal or vertical salinity and inclined temperature gradients to studying the influence of the Soret effect on the dichotomy in a similar model. Only longitudinal modes are considered. We treat first normal modes and analyze the influence of the Soret effect on the critical values of the vertical thermal Rayleigh number, $R_{\rm v}$, wavenumber, l, and frequency, ω, for a variety of values of the horizontal thermal Rayleigh number $R_{\rm h}$, and the vertical salinity Rayleigh number, $S_{\rm v}$. Our results for normal modes agree well with relevant results of Narayana et al. (J. Fluid Mech. 612:1–19, 2008) obtained for a similar model in a different context. In the computations, we use a high-precision pseudo-spectral Chebyshev-collocation method. Further, we apply the formalism of absolute and convective instabilities and compute the group velocity of the unstable wave-packet emerging in a marginally unstable state to determine the nature of the instability at the onset of convection. The influence of the Soret effect on the absolute/convective instability dichotomy present in the model is treated by considering the destabilization for seven values of the Soret number: $S_{\rm r} = -1, -0.5, -0.1, 0, 0.1, 0.5, 1$, for all the parameter cases in the treatment of normal modes.

Keywords Porous layer · Inclined thermal and vertical solutal gradients · Soret-driven thermosolutal convection · Absolute/convective instability dichotomy

L. Brevdo (✉)
Institut de Mécanique des Fluides et des Solides, Université de Strasbourg/CNRS,
2 rue Boussingault, 67000 Strasbourg, France
e-mail: brevdo@unistra.fr

O. A. Cirpka
Center for Applied Geoscience, Eberhard Karls Universität Tübingen, Tübingen, Germany

1 Introduction

Since the publication of a seminal work of Weber (1974) on the convection in a porous layer induced by horizontal and vertical thermal gradients, the subject of natural and forced convection in a porous medium including the thermohaline convection received a considerable attention in the literature owing to a great variety of applications, see Bear (1972), Guo and Kaloni (1995), Nield (1991), Nield (1994), Nield (1998), Nield and Bejan (2006), Nield et al. (1993), Manole et al. (1994), Qiao and Kaloni (1997, 1998), Sarkar and Phillips (1992), Straughan (2004), Straughan and Walker (1996) for reviews and references.

The Soret effect describes mass separation in a salt solution with a non-uniform temperature distribution. This effect was also intensively studied in the literature in relation to the emergence of convection in a porous medium, see e.g., Bahloul et al. (2003), Marcoux and Charrier-Mojtabi (1998), Narayana et al. (2008), Sovran et al. (2001) for reviews and references. The phenomenon of mass separation in a salt solution in the presence of a temperature gradient, known today under the name the Soret effect, was first observed and reported by Ludwig (1856) and further described and studied rather in detail by Soret (1879). In an experiment with a salt solution under a temperature gradient, it was observed that the salt was more concentrated near the cold end of the experimental tube. The conclusion was that a flux of salt resulted owing to the temperature gradient. Under steady-state conditions, the mass flux due to the Soret effect must be balanced, in the aforementioned experiments, by a diffusive mass flux, resulting in a steady-state concentration gradient. The Soret effect is of significance in many natural systems and for human activities including the microstructure of the ocean, the convection in stars, the transport across membranes induced by small thermal gradients in living tissues, the operation of solar ponds, and the oil exploration, see e.g., Platten et al. (2007) for a review. Formally, the Soret effect is expressed by the presence of a thermal diffusion term in the concentration balance equation. For references and a review of experimental results for the Soret effect see Platten (2006).

In this article, we analyze the influence of the Soret effect on the nature of flow destabilization in a simple model of a saturated horizontally extended porous layer, using the approach of absolute and convective instabilities. In this approach, the response of a linearly unstable model to a perturbation that is initially localized in space is studied. The response to such a realistic perturbation has the form of a wavepacket. Hereby two different complementary scenarios of the spatio-temporal evolution of the wavepacket are possible. In the first scenario, the wavepacket grows linearly in the entire flow domain thus destroying eventually the base flow throughout the domain due to nonlinear effects. This is the case of absolute instability. In the alternative scenario, the growing wavepacket propagates away from the location of the initial perturbation, leaving behind an unperturbed base state at every fixed point in the flow domain. In this case, the flow is said to be convectively unstable, but absolutely stable.

In Fig. 1, we present a schematic one-dimensional illustration of the spatio-temporal evolution of the amplitude of an unstable disturbance in the absolutely unstable case and in the convectively unstable, but absolutely stable case. The solid lines show schematically

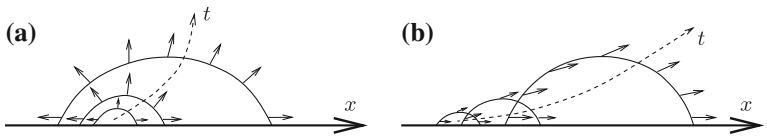

Fig. 1 **a** Absolute instability; **b** convective instability

the growth and spreading in space with time of the wavepacket amplitude, and the dashed line illustrates the trajectory of the peak of the wavepacket. While in the absolutely instable case the unstable disturbance propagates and spreads into all directions, it affect only so to say "downstream" regions in the convectively unstable, but absolutely stable case, i.e., the regions in the direction of increasing x in Fig. 1. Until recently, the emergence of convection in porous media has been analyzed by the approach of monochromatic perturbations. In comparison to this approach, the advantage of the approach of absolute and convective instabilities is that it provides an important information concerning the evolution of realistic perturbations in unstable flow. Specifically, (i) an unstable wavepacket propagates with the group velocity whereas sinusoidal disturbances propagate with the phase speed that can be different in both its magnitude and its direction from the group velocity, (ii) a convectively unstable, but absolutely stable state can be viewed as representing a physical end state in a certain part of the flow domain depending on the spatio-temporal evolution characteristics of the convectively unstable wavepacket in the flow, whereas an unstable monochromatic wave is unstable at every point in the flow domain.

To illustrate the difference between the evolution of localized disturbances in the absolutely unstable case and in the absolutely stable, but convectively unstable case we give here an example which is a slightly modified shortened reproduction of an analytic example presented in Brevdo and Bridges (1996).

1.1 Illustrative Example

We consider the linear convection–diffusion equation subject to the first-order increase of the solute concentration:

$$\frac{\partial c}{\partial t^*} = D^* \frac{\partial^2 c}{\partial x^{*2}} + v^* \frac{\partial c}{\partial x^*} + \lambda^* c, \tag{1}$$

where c, t^*, and x^* are the concentration, time, and length, respectively, and D^*, v^*, and λ^* are positive constants. Here and further in the text, the superscript asterisk, when used, denotes dimensional quantities. By using in this example the diffusive time scaling,

$$t = \frac{t^* D^*}{L^{*2}}, \quad x = \frac{x^*}{L^*}, \tag{2}$$

with L^* denoting a characteristic length scale, Eq. (1) can be written as

$$\frac{\partial c}{\partial t} = \frac{\partial^2 c}{\partial x^2} + Pe \frac{\partial c}{\partial x} + Da\, c, \tag{3}$$

where

$$Pe = \frac{v^* L^*}{D^*} \quad \text{and} \quad Da = \frac{\lambda^* L^{*2}}{D^*} \tag{4}$$

are the Péclet and Damköhler numbers, respectively. We treat stability of the trivial state, $c(x, t) = 0$. A normal-mode substitution,

$$c(x, t) = c_0\, \mathrm{e}^{\mathrm{i}(kx - \omega t)}, \tag{5}$$

gives the dispersion relation:

$$\omega = -Pe\, k + \mathrm{i}\left(Da - k^2\right). \tag{6}$$

Hence, $\mathrm{Im}\,\omega = \omega_{\mathrm{i}}(k) = Da - k^2$, for real k. As $Da > 0$, it follows that the base state is linearly unstable, for all the values of Pe, and with this the analysis of normal modes is complete. However, the normal-mode approach provides no information concerning the evolution of localized disturbances, for different values of Pe and Da.

To illustrate the influence of the values of Pe and Da on the dynamics of localized disturbances we treat an initial-value problem for Eq. (3) in a particular case when at $t = 0$ the initial data for (3) is a Gaussian pulse of unit amplitude,

$$c(x,t)\big|_{t=0} = \mathrm{e}^{-bx^2/4}, \quad b > 0. \tag{7}$$

For such an initial data, the exact solution of (3), for all $-\infty < x < \infty$ and all $t \geq 0$, is

$$\begin{aligned} c(x,t) = \frac{\exp(Da\,t)}{\sqrt{1+bt}} \exp\left[-\frac{b(x+Pe\,t)^2}{4(1+bt)}\right] = \frac{1}{\sqrt{1+bt}} \\ \times \exp\left\{\frac{t}{1+bt}\left[Da + bt\left(Da - \frac{Pe^2}{4}\right)\right]\right\} \exp\left[-\frac{b(x^2+2Pe\,xt)}{4(1+bt)}\right]. \end{aligned} \tag{8}$$

If $Pe > 2\sqrt{Da}$ the solution decays exponentially to zero at any fixed x, as $t \to \infty$. However, for any value of Pe, in a frame of reference moving at speed $(-Pe)$ with respect to the absolute frame of reference, that is $x = x_0 - Pe\,t$, where x_0 is an arbitrary fixed number, the solution (8) grows exponentially in time. This means that when $Pe > 2\sqrt{Da}$ the instability in the absolute frame of reference is localized in space. Hence, for the values of Pe and Da satisfying the inequality $Pe/\sqrt{Da} > 2$ the base state is absolutely stable, but convectively unstable. On the other hand, if $Pe/\sqrt{Da} < 2$ there is an exponential growth of the solution (8) in time at every fixed position, x, in the absolute frame of reference. Therefore, in such a case the base state is absolutely unstable. When $Pe/\sqrt{Da} = 2$, at each fixed location, x, the solution (8) decays algebraically as $1/\sqrt{bt}$, for growing t. Thus, as $Pe/\sqrt{Da}$ decreases passing through the value of $Pe/\sqrt{Da} = 2$, a transition from the convective to absolute instability occurs.

The distinction between these two types of instabilities illustrated in the above example is of fundamental importance in applications. Localized instability convects away from a region where the triggering disturbances originate and, presumably, it may be possible to control. An absolute or global instability has generally a catastrophic character as it grows exponentially in time at all the points in space destroying the base state throughout in the absolute frame of reference.

Also, the nature of the linear destabilization is assumed to influence the fundamental features of the emerging fully developed nonlinear state that, according to the assumption, are essentially different in the case of the destabilization through absolutely instability from those in the case when at the destabilization the state is absolutely stable, but convectively unstable. The formalism of absolute and convective instabilities and spatially amplifying waves for spatially uniform two-dimensional flows was developed in its modern form in the plasma physics literature (see Briggs 1964, Bers 1973). The formalism was extended to three-dimensional homogeneous flows by Brevdo (1991) and to spatially developing two-dimensional flows by Brevdo (2002, 2003, 2004, 2005).

An analysis of the character of localized perturbations at the onset of convection in a model of flow in a saturated porous layer with inclined temperature gradient and vertical throughflow was performed by Brevdo (2009) and Brevdo and Ruderman (2009a,b) by using the methods of absolute and convective instabilities. The treatment in those works was recently extended by Diaz and Brevdo (2011, 2012) to a model of a saturated porous layer with either horizontal or vertical salinity and inclined thermal gradients, and horizontal throughflow.

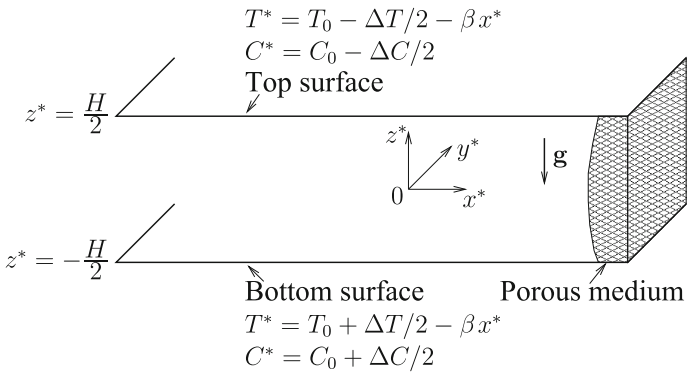

Fig. 2 Schematics of the problem

In those studies, an absolute/convective instability dichotomy at the onset of convection was found in the set of the exact solutions for the equations of motion depending on the physical parameters involved.

In this article, we analyze the influence of the Soret effect on the nature of destabilization—through absolute or convective instability—of longitudinal disturbances in a saturated horizontally extended porous layer subjected to inclined thermal and vertical salinity gradients. The model we use is closely related to the one treated in the article of Narayana et al. (2008), further in the text referred to as NMG, where extensive computations of the influence of the Soret effect on the normal-mode stability were performed.

The article is organized as follows. In Sect. 2, we sketch the model, review the non-dimensional governing equations, and present the steady-state base solution. Section 3 gives a description of an initial-value problem for small disturbances and the solution of the problem in the form of an inverse Laplace-Fourier integral. In Sect. 4, the procedure for treating the transition from convective to absolute instability is described. Section 5 presents the numerical results, and Section 6 contains conclusions.

2 Formulation and Steady-State Solution

The model we treat is similar to the model considered by NMG. We give here a concise description of the model by using the setting, notations and non-dimensionalization of that article.

2.1 Formulation

We consider a flow in a horizontal homogeneous extended saturated porous layer of height H bounded by two horizontal impermeable, solid surfaces with fixed constant temperature and concentration, and driven by inclined thermal and vertical salinity gradients under the influence of the Soret effect. The Cartesian axes are chosen with the origin at the mid-height of the layer and with the z^*-axis pointing vertically upwards. The horizontal component of the thermal gradients, β, is supposed to be pointing in the direction opposite to the positive direction of the x^*-axis. The imposed vertical temperature difference and vertical concentration difference are ΔT and ΔC, respectively, across the height of the domain. We assume that the flow in the porous medium is governed by Darcy's law and the Oberbeck-Boussinesq approximation can be applied, see Bear (1972). Figure 2 presents a schematic illustration

of the physical situation considered. We analyze the nature of the destabilization of two-dimensional longitudinal disturbances. For such disturbances, the perturbation flow field is independent of x.

By using the non-dimensionalization applied in NMG,

$$\begin{gathered}(x, y, z) = (x^*, y^*, z^*)/H, \quad t = t^* \frac{\alpha_\mathrm{m}}{aH^2}, \quad \mathbf{v} = \mathbf{v}^* \frac{H}{\alpha_\mathrm{m}}, \quad P = \frac{K(P^* + \rho_0 g z^*)}{\mu \alpha_\mathrm{m}}, \\ T = (T^* - T_0) \frac{\rho_0 g \gamma_\mathrm{T} K H}{\mu \alpha_\mathrm{m}}, \quad C = (C^* - C_0) \frac{\rho_0 g \gamma_\mathrm{C} K H}{\mu D_\mathrm{m}},\end{gathered} \tag{9}$$

the governing dimensionless equations for the flow can be written as

$$\begin{gathered}\nabla \cdot \mathbf{v} = 0, \\ \nabla P + \mathbf{v} - \left(T + \frac{1}{Le} C\right) \mathbf{k} = 0, \\ \frac{\partial T}{\partial t} + \mathbf{v} \cdot \nabla T = \nabla^2 T, \\ \frac{\phi}{a} \frac{\partial C}{\partial t} + \mathbf{v} \cdot \nabla C = \frac{1}{Le} \nabla^2 C + S_\mathrm{r} \nabla^2 T, \\ -\infty < x, y < \infty, \quad -1/2 < z < 1/2, \quad t > 0.\end{gathered} \tag{10}$$

The dimensionless boundary conditions are

$$w = 0, \quad T = \mp R_\mathrm{v}/2 - R_\mathrm{h} x, \quad C = \mp S_\mathrm{v}/2 \ \text{ at } \ z = \pm 1/2. \tag{11}$$

In (10) and (11), ∇ is the dimensionless gradient operator, $\mathbf{k} = (0, 0, 1)^T$, and $\mathbf{v} = (u, v, w)^T$, t, P, T, and C are the Darcy velocity vector, time, pressure, temperature and concentration, respectively. The dimensionless parameters appearing in the governing equations and the boundary conditions are the Lewis number, Le, the vertical thermal Rayleigh number, R_v, the horizontal thermal Rayleigh number, R_h, the vertical solutal Rayleigh number, S_v, and the Soret number, S_r, given by

$$\begin{gathered}Le = \frac{\alpha_\mathrm{m}}{D_\mathrm{m}}, \quad R_\mathrm{v} = \frac{\rho_0 g \gamma_\mathrm{T} K H \Delta T}{\mu \alpha_\mathrm{m}}, \quad R_\mathrm{h} = \frac{\rho_0 g \gamma_\mathrm{T} K H^2 \beta_\mathrm{T}}{\mu \alpha_\mathrm{m}}, \\ S_\mathrm{v} = \frac{\rho_0 g \gamma_\mathrm{C} K H \Delta C}{\mu D_\mathrm{m}} \quad \text{and} \quad S_\mathrm{r} = \frac{D_\mathrm{m} k_\mathrm{m} \Delta T S_\mathrm{v}}{c_\mathrm{s} c_\mathrm{p} \alpha_\mathrm{m} \Delta C R_\mathrm{v}},\end{gathered} \tag{12}$$

with

$$\alpha_\mathrm{m} = \frac{k_\mathrm{m}}{(\rho c_\mathrm{p})_\mathrm{f}} \quad \text{and} \quad a = \frac{(\rho \mathrm{c})_\mathrm{m}}{(\rho c_\mathrm{p})_\mathrm{f}}. \tag{13}$$

In (9), (12), and (13), g is the gravity acceleration, μ, ρ, c_s, and c_p denote the viscosity, density, concentration susceptibility, and specific heat at constant pressure, respectively, K is the permeability and ϕ is the porosity of the porous medium, k_m and D_m denote the thermal conductivity and, correspondingly, solutal diffusivity of the medium, γ_T and γ_C are the thermal and, respectively, solutal expansion coefficients of the fluid, and the subscripts m, f, and 0 refer to the porous medium, the fluid, and the uniform reference state, respectively.

2.2 Steady-State Solution

When there is no net flow in the horizontal direction problem, the system of equation (10), (11) admits a steady-state uni-directional flow solution of the form

$$\begin{gathered} u = U_{\mathrm{s}}(z),\ v = 0,\ \ w = 0,\ \ P = P_{\mathrm{s}}(x, y, z), \\ T = T_{\mathrm{s}}(z) - R_{\mathrm{h}} x,\ \ C = C_{\mathrm{s}}(z), \end{gathered} \tag{14}$$

which is a partial case of the solution given by NMG. The functions U_{s}, T_{s}, and C_{s} can be expressed as

$$\begin{gathered} U_{\mathrm{s}} = R_{\mathrm{h}} z,\ \ T_{\mathrm{s}} = -R_{\mathrm{v}} z + \frac{R_{\mathrm{h}}^2}{24}(z - 4z^3), \\ C_{\mathrm{s}} = -S_{\mathrm{v}} z + \frac{Le S_{\mathrm{r}} R_{\mathrm{h}}^2}{24}(4z^3 - z). \end{gathered} \tag{15}$$

3 Initial-Value Problem

An initial-value problem for a two-dimensional longitudinal perturbation flow in the model is derived by perturbing the base state and linearizing the governing equations. We write $\mathbf{v} = (U_{\mathrm{s}}, 0, 0)^T + \mathbf{v}'$, with $\mathbf{v}' = (0, v', w')^T$, $T = T_{\mathrm{s}} - R_{\mathrm{h}} x + \theta'$, $C = C_{\mathrm{s}} + c'$, and $P = P_{\mathrm{s}} + p'$, where v', w', θ', c', and p' are small perturbations, substitute the perturbed quantities into (10) and (11), and neglect the products of the perturbation terms to obtain

$$\begin{gathered} \frac{\partial v'}{\partial y} + \frac{\partial w'}{\partial z} = 0, \\ \frac{\partial p'}{\partial y} + v' = m_{\mathrm{y}}, \\ \frac{\partial p'}{\partial z} + w' - \left(\theta' + \frac{1}{Le} c'\right) = m_{\mathrm{z}}, \\ \frac{\partial \theta'}{\partial t} + \frac{\mathrm{d}T_{\mathrm{s}}}{\mathrm{d}z} w' = \nabla^2 \theta' + e, \\ \frac{\phi}{a}\frac{\partial c'}{\partial t} + \frac{\mathrm{d}C_{\mathrm{s}}}{\mathrm{d}z} w' = \frac{1}{Le}\nabla^2 c' + S_{\mathrm{r}} \nabla^2 \theta' + s, \\ -1/2 < z < 1/2, \quad -\infty < y < \infty, \quad t > 0, \\ (v', w', p', \theta', c')|_{t=0} = (v_0, w_0, p_0, \theta_0, c_0)(z, y), \\ (v', w', p', \theta', c') = (v_1, w_1, p_1, \theta_1, c_1)(y, t) \ \text{ at } \ z = -1/2, \\ (v', w', p', \theta', c') = (v_2, w_2, p_2, \theta_2, c_2)(y, t) \ \text{ at } \ z = 1/2, \end{gathered} \tag{16}$$

where now $\nabla = (\partial/\partial y, \partial/\partial z)^T$, and $(m_{\mathrm{y}}, m_{\mathrm{z}})$, e, and s denote the sources of momentum energy, and salinity, respectively. It is assumed on physical grounds that the source functions and the perturbation functions on the boundaries have finite support in y and t, and the functions appearing in the initial conditions have finite support in y. Further in the text, except for the normal-mode expansion given by (21), we omit the prime denoting the perturbation quantities for convenience.

We eliminate v and p from the first three equations in (16) to obtain a system of three equations for w, θ, and c that can be written as

$$\begin{aligned}\left(\frac{\partial^2}{\partial y^2}+\frac{\partial^2}{\partial z^2}\right)w-\frac{\partial^2\theta}{\partial y^2}-\frac{1}{Le}\frac{\partial^2 c}{\partial y^2}&=\frac{\partial}{\partial y}\left(\frac{\partial m_z}{\partial y}-\frac{\partial m_y}{\partial z}\right),\\ \frac{\mathrm{d}T_s}{\mathrm{d}z}w+\left(\frac{\partial}{\partial t}-\frac{\partial^2}{\partial y^2}-\frac{\partial^2}{\partial z^2}\right)\theta&=e,\\ \frac{\mathrm{d}C_s}{\mathrm{d}z}w-S_\mathrm{r}\left(\frac{\partial^2}{\partial y^2}+\frac{\partial^2}{\partial z^2}\right)\theta+\left[\frac{\phi}{a}\frac{\partial}{\partial t}-\frac{1}{Le}\left(\frac{\partial^2}{\partial y^2}+\frac{\partial^2}{\partial z^2}\right)\right]c&=s.\end{aligned}\tag{17}$$

The initial-value problem for the system (17) is solved by using the combined Fourier-Laplace transform. Its solution is similar to that of a similar problem described by Diaz and Brevdo (2012). The vertical component of the perturbation velocity, $w = w(z, y, t)$, of the solution of the initial-value problem (16) can be expressed as

$$w(z,y,t)=\frac{1}{4\pi^2}\int_{\mathrm{i}\sigma-\infty}^{\mathrm{i}\sigma+\infty}\int_{-\infty}^{\infty}\frac{T(z,l,\omega)}{D(l,\omega)}\,\mathrm{e}^{\mathrm{i}(ly-\omega t)}\mathrm{d}l\,\mathrm{d}\omega,\tag{18}$$

where l is a wavenumber (and a Fourier transform parameter) and ω is a frequency (and a Laplace transform parameter). In (18), $D(l, \omega)$ is the dispersion–relation function of the problem as it is defined in the normal-mode approach, see Drazin and Reid (1989), the function $T(z, l, \omega)$ is a linear combination of the transforms of the source functions, of the perturbation functions on the boundaries and of the functions appearing in the initial conditions and, hence, this function is in a certain sense arbitrary, and σ is a real number that is greater than the maximum growth rate of the normal modes, σ_m :

$$\sigma > \sigma_\mathrm{m} = \max\{\mathrm{Im}\,\omega \mid D(l,\omega)=0,\ \mathrm{Im}\,l=0\}.\tag{19}$$

4 Destabilization Through Either Absolute or Convective Instability

A procedure for determining the nature of instability—absolute or convective—at the point of destabilization is described in Brevdo (2009). The procedure originates from the mathematical formalism of absolute and convective instabilities and is related to the collision criterion for determining the nature of instability of an unstable flow, see Briggs (1964). For a marginally unstable state, technically the procedure is based on computing the group velocity of the emerging unstable wavepacket. In a two-dimensional case, the group velocity is given by

$$V_\mathrm{g}=\frac{\mathrm{d}\omega_\mathrm{r}(l_\mathrm{c})}{\mathrm{d}l},\tag{20}$$

where l_c is the critical wavenumber, meaning that $\omega_\mathrm{i}(l_\mathrm{c})$ is marginally greater than zero. Here and further in the text the subscript r denotes the real part and the subscript i denotes the imaginary part of a complex number. When the group velocity $V_\mathrm{g} = 0$ the destabilization in our case of longitudinal disturbances has the character of absolute instability. When $V_\mathrm{g} \neq 0$ and $|V_\mathrm{g}|$ is large enough the flow at the onset of convection is absolutely stable, but convectively unstable.

In the numerical treatment, we computed the critical values of the marginally unstable state, in every parameter case considered, and calculated the group velocity by using Eq. (20). In all the computations, there was either $V_\mathrm{g} = 0$ or $|V_\mathrm{g}|$ was large enough. Hence, a conclusion concerning the nature of the destabilization was unequivocally drawn in every case treated.

5 Numerical Procedure

For analyzing the stability of the model, we substitute the normal-mode expansion,

$$\left[w', \theta', c'\right] = [w(z), \theta(z), c(z)] \times \exp[\mathrm{i}(ly - \omega t)], \tag{21}$$

into the homogeneous system corresponding to system (17), i.e. the one with $m_y = m_z = e = s = 0$, to obtain a system of equations for the perturbation amplitudes $w(z)$, $\theta(z)$, and $c(z)$:

$$\begin{gathered}
\left(\frac{\mathrm{d}^2}{\mathrm{d}z^2} - l^2\right) w + l^2\theta + \frac{l^2}{Le} c = 0, \\
\frac{\mathrm{d}T_s}{\mathrm{d}z} w - \left(\frac{\mathrm{d}^2}{\mathrm{d}z^2} - l^2 + \mathrm{i}\omega\right) \theta = 0, \\
\frac{\mathrm{d}C_s}{\mathrm{d}z} w - S_\mathrm{r} \left(\frac{\mathrm{d}^2}{\mathrm{d}z^2} - l^2\right) \theta - \left(\frac{1}{Le}\frac{\mathrm{d}^2}{\mathrm{d}z^2} - \frac{l^2}{Le} + \frac{\mathrm{i}\phi}{a}\omega\right) c = 0, \\
-1/2 < z < 1/2.
\end{gathered} \tag{22}$$

The boundary conditions for the amplitudes on the horizontal impermeable, isosolutal, isothermal boundaries read as

$$w = \theta = c = 0 \ \text{ at } \ z = \pm 1/2. \tag{23}$$

Equation (22) together with the boundary conditions (23) constitute a differential eigenvalue problem. In the stability analysis of normal modes, the frequency ω in this problem, for a given wavenumber, l, appears as an eigenvalue parameter. Hereby, one is interested in computing all the pairs, (l, ω), with real l, such that the eigenvalue problem (22), (23) has a non-trivial solution and to establish the conditions based on the sign of ω_i under which the steady state is destabilized. In this article, we are looking for the critical values of R_v, for several combinations of other five parameters, Le, (ϕ/a), R_h, S_v, and S_r, in the problem, whereby a special attention is given to the influence of the Soret number, S_r, on the destabilization. The differential eigenvalue problem is treated numerically by applying a discretization using a pseudo-spectral Chebyshev collocation method. The resulting generalized algebraic eigenvalue problem for ω is solved using the global IMSL solver DGVLCG. The details of the numerical treatment of a similar problem are given in the appendix of Diaz and Brevdo (2011).

6 Stability Results for Normal Modes

An extensive stability analysis of normal modes in a similar model, but in a somewhat different context, was performed by NMG who employed the two-term Galerkin method in a way similar to that proposed in the study of Nield et al. (1993). In this section, we present in a sequel of tables our stability results for longitudinal normal modes including the critical values of wavenumber and of frequency. In the computations of the critical values in this section and of the values of the group velocity in Sect. 7, it was established that 35 collocation points are sufficient for attaining the apparent relative error of <0.05 % in all the cases treated.

To analyze the influence of the Soret effect on the destabilization, we select the values 0, 10, 20, 30, 40, 50, 60 for R_h, the values -30, -20, -10, 0, 10, 20, 30 for S_v, and the values -1, -0.5, -0.1, 0, 0.1, 0.5, 1 for S_r. Throughout the computations the Lewis number, Le, is kept at 10 and $\phi/a = 1$, see Manole et al. (1994).

Table 1 Values of the critical vertical thermal Rayleigh number, R_{vc}, for various values of the solutal Rayleigh number, S_v, and the Soret number, S_r, for $R_h = 0$

	$S_v = -30$	-20	-10	0	10	20	30
$S_r = -1$	34.739	29.739	24.739	19.739	14.738	9.7392	4.7392
-0.5	46.319	39.652	32.986	26.319	19.652	12.986	6.3189
-0.1	46.427	45.427	44.427	35.889	26.799	17.708	8.6167
0	46.427	45.427	44.427	39.479	29.479	19.479	9.4784
0.1	46.427	45.427	44.427	43.427	32.754	21.643	10.532
0.5	46.427	45.427	44.427	43.427	42.427	38.957	18.957
1	46.427	45.427	44.427	43.427	42.427	41.427	40.427

Table 2 Values of the critical oscillatory frequency, $\omega_{rc} = \omega_r(l_c)$, for various values of S_v and S_r, for $R_h = 0$

	$S_v = -30$	-20	-10	0	10	20	30
$S_r = -1$	0	0	0	0	0	0	0
-0.5	0	0	0	0	0	0	0
-0.1	4.2617	3.0629	0.77546	0	0	0	0
0	4.7689	3.7241	2.2325	0	0	0	0
0.1	5.2271	4.2831	3.0606	0.62408	0	0	0
0.5	6.7559	6.0225	5.1864	4.1864	2.8555	0	0
1	8.2791	7.6602	6.9866	6.2408	5.3928	4.3837	3.0579

6.1 Case with Zero Horizontal Temperature Gradient, $R_h = 0$

The results for this case are presented in Tables 1, 2, and 23. The results for the critical wavenumber, for all the cases, are presented in the tables given in the Appendix. As seen from the results presented in Table 1, the value of the critical vertical thermal Rayleigh number, R_{vc}, is a decaying function of the solutal Rayleigh number, S_v, for each fixed value of the Soret number, S_r, and a non-decaying function of S_r, for each fixed value of S_v. The value of l_c, shown in Table 23 varies slightly with S_v, for $S_r = -1$ and is constant, for $S_r \geq -0.5$, for all the values of S_v considered. For $S_r = -1, -0.5$, the critical oscillatory frequency, ω_{rc}, shown in Table 2 is nil, for all the values of S_v. Similarly, for $-0.2 \leq S_r \leq 0.5$, the critical modes are non-oscillatory, for S_v sufficiently large in each case considered. In the oscillatory cases, ω_{rc} decays as a function of S_v and grows with S_r. A comparison of the critical values of R_v, for the non-oscillatory modes in Table 1(a) in NMG with the corresponding values in Table 1 in this article shows good agreement, for all the cases. For this value of R_h, the values of R_{vc} in Table 1 agree very well with the values obtained by using the analytic expressions in Eqs. (28) and (29) in NMG, for the non-oscillatory and, respectively, oscillatory cases. For instance, for $S_v = -30$, $S_r = -1$, the computed value is $R_{vc} = 34.73921388$, whereas the value given by Eq. (28) in NMG is $R_{vc}^{NMG} = 34.73920880$. Hence, the relative deviation of the computed R_{vc} from R_{vc}^{NMG} is $\delta = |R_{vc} - R_{vc}^{NMG}|/R_{vc} = 0.0000146\,\%$.

6.2 Case for a Horizontal Thermal Rayleigh Number, $R_h = 10$

In this case, the critical vertical thermal Rayleigh number, R_{vc}, decays as a function of the Soret number, S_v, for each fixed value of the solute Rayleigh number, S_r, considered, but the

Table 3 Values of the critical vertical thermal Rayleigh number, R_{vc}, for various values of S_v and S_r, for $R_h = 10$

	$S_v = -30$	-20	-10	0	10	20	30
$S_r = -1$	49.650	44.650	39.650	34.650	29.650	24.650	19.650
-0.5	50.217	49.217	43.852	37.185	30.519	23.852	17.185
-0.1	49.206	48.206	47.206	40.710	31.619	22.528	13.437
0	48.956	47.956	46.956	42.008	32.008	22.008	12.008
0.1	48.706	47.706	46.706	43.583	32.472	21.361	10.250
0.5	47.712	46.713	45.715	44.718	36.006	16.006	-3.9939
1	46.479	45.483	44.489	43.495	42.503	-594.08	-1594.08

Table 4 Values of the critical oscillatory frequency, $\omega_{rc} = \omega_r(l_c)$, for various values of S_v and S_r, for $R_h = 10$

	$S_v = -30$	-20	-10	0	10	20	30
$S_r = -1$	0	0	0	0	0	0	0
-0.5	3.2103	1.3878	0	0	0	0	0
-0.1	4.5124	3.4041	1.6775	0	0	0	0
0	4.7674	3.7242	2.2334	0	0	0	0
0.1	5.0037	4.0079	2.6627	0	0	0	0
0.5	5.8056	4.9324	3.8668	2.3607	0	0	0
1	6.5791	5.7724	4.8437	3.6876	1.9310	0	0

dependence of R_{vc} on S_r is mixed depending on the value of S_v, as seen from Table 3. For instance, for $S_v = 10$, the value of R_{vc} grows with S_r, but for $S_v = 20$ and 30 it decays when S_r grows. The value of l_c presented in Table 24 does not vary significantly either with S_v or with S_r.

The dependence of ω_{rc} presented in Table 4 on S_v and S_r is qualitatively similar to that in the case $R_h = 0$. However, the domain of non-oscillatory parameter cases is modified. Particularly, for $S_r = 1$, there are two non-oscillatory cases with $S_v = 20$ and 30. According to Eq. (28) in NMG for the non-oscillatory cases, in such cases the value of R_{vc} has a singularity, i.e. it is infinite, at the point $S_r = 1$. We observed this singularity numerically. Specifically, when $S_r \to 0^-$, the numerically evaluated value of R_{vc} tends to $-\infty$. Hence, in such cases as well as in similar cases, with $R_h \geq 20$, we computed the value of R_{vc} putting $S_r = 0.99$. The singularity in these computations is manifested by large negative values of R_{vc}, with $|R_{vc}|$ that are by up to two orders of magnitude larger than the corresponding values in the non-singular cases. For $R_h = 10$, the approximation provided by the Eqs. (28) and (29) in NMG for the numerically evaluated value of R_{vc} is still good; however, it is much weaker than that in the case $R_h = 0$. For instance, for $S_v = -30$, $S_r = -1$, the computed value is $R_{vc} = 49.65028363$, whereas the value given by the Eq. (28) in NMG is $R_{vc}^{NMG} = 49.93738635$. Hence, the relative deviation is $\delta = |R_{vc} - R_{vc}^{NMG}|/R_{vc} = 0.578\,\%$ which is considerably larger than the relative deviation of $0.0000146\,\%$ in the corresponding case, with $R_h = 0$. Further weakening of the approximation by both Eqs. (28) and (29) in NMG is observed at each stage when R_h increases.

Table 5 Values of the critical vertical thermal Rayleigh number, R_{vc}, for various values of S_v and S_r, for $R_h = 20$

	$S_v = -30$	-20	-10	0	10	20	30
$S_r = -1$	66.829	65.855	64.885	63.920	62.960	62.009	58.778
-0.5	61.496	60.496	59.496	58.496	57.496	54.939	48.272
-0.1	57.470	56.467	55.464	54.460	45.890	36.799	27.708
0	56.499	55.499	54.498	49.549	39.549	29.549	19.549
0.1	55.542	54.547	53.552	42.738	31.627	20.516	9.4051
0.5	45.350	25.350	5.3497	-14.650	-34.650	-54.650	-74.650
0.99	-3662.4	-4662.4	-5662.4	-6662.4	-7662.4	-8662.4	-9662.4

Table 6 Values of the critical oscillatory frequency, $\omega_{rc} = \omega_r(l_c)$, for various values of S_v and S_r, for $R_h = 20$

	$S_v = -30$	-20	-10	0	10	20	30
$S_r = -1$	6.8456	6.2399	5.5648	4.8013	3.8968	2.7120	0
-0.5	6.2985	5.6024	4.7909	3.8202	2.4971	0	0
-0.1	5.1907	4.2600	3.0586	0.75283	0	0	0
0	4.7769	3.7274	2.2353	0	0	0	0
0.1	4.2750	3.0451	0.51503	0	0	0	0
0.5	0	0	0	0	0	0	0
0.99	0	0	0	0	0	0	0

6.3 Case for a Horizontal Thermal Rayleigh Number, $R_h = 20$

The results for this case are presented in Tables 5, 6, and 25. In this case, the value of R_{vc} is a decaying function of both S_v and S_r. The critical wavenumber, l_c, varies slightly with S_v, for each fixed value of $S_r = -1, -0.1$, and -0.5, and does not depend on S_v, for each fixed value of $S_r \geq 0$. The domain of the non-oscillatory modes occupies now a portion of Table 6 laying roughly below the diagonal from the lower left-hand side corner to the upper right-hand side corner of the table, whereas in the cases $R_h = 0$ and 10, the corresponding domain in Tables 2 and 4, respectively, lies roughly above the diagonal from the upper left-hand side corner to the lower right-hand side corner. In contrast to the cases $R_h = 0$ and 10 the critical oscillatory frequency, ω_{rc}, decreases with both S_v and S_r. For $S_r = 1$, all the modes are non-oscillatory, hence, the computation of R_{vc} for $S_r = 0.99$ produced very large negative values in the bottom line of Table 6.

6.4 Case for a Horizontal Thermal Rayleigh Number, $R_h = 30$

In this case, similar to the case $R_h = 20$, the value of R_{vc} presented in Table 7 is a decaying function of both S_v and S_r. The value of l_c shown in Table 26 increases with S_r for every fixed S_v, varies slightly with S_v for each fixed $S_r \leq -0.1$ and remains constant for each fixed $S_r \geq 0$. The domain of non-oscillatory cases presented in Table 8, although slightly modified compared to that in the case $R_h = 20$, remains roughly below the diagonal from the lower left-hand side corner to the upper right-hand side corner of the table. Like in the case $R_h = 20$, in the oscillatory cases, the critical oscillatory frequency, ω_{rc}, decreases with

Table 7 Values of the critical vertical thermal Rayleigh number, R_{vc}, for various values of S_v and S_r, for $R_h = 30$

	$S_v = -30$	-20	-10	0	10	20	30
$S_r = -1$	92.452	91.522	90.597	89.680	88.769	87.868	86.976
-0.5	80.040	79.044	78.049	77.054	76.060	75.066	74.074
-0.1	70.996	69.983	68.968	67.949	66.927	59.889	50.798
0	68.916	67.915	66.913	61.957	51.957	41.957	31.957
0.1	66.958	63.551	52.440	41.328	30.217	19.106	7.9951
0.5	-78.591	-98.591	-118.59	-138.59	-158.59	-178.59	-198.59
0.99	-18747	-19747	-20747	-21747	-22747	-23747	-24747

Table 8 Values of the critical oscillatory frequency, $\omega_{rc} = \omega_r(l_c)$, for various values of S_v and S_r, for $R_h = 30$

	$S_v = -30$	-20	-10	0	10	20	30
$S_r = -1$	10.232	9.8399	9.4189	8.9790	8.5307	8.0567	7.5608
-0.5	9.0197	8.5375	8.0237	7.4868	6.9002	6.2626	5.5513
-0.1	6.1300	5.3594	4.4591	3.3301	1.5044	0	0
0	4.7972	3.7432	2.2433	0	0	0	0
0.1	2.6352	0	0	0	0	0	0
0.5	0	0	0	0	0	0	0
0.99	0	0	0	0	0	0	0

Table 9 Values of the critical vertical thermal Rayleigh number, R_{vc}, for various values of S_v and S_r, for $R_h = 40$

	$S_v = -30$	-20	-10	0	10	20	30
$S_r = -1$	-1.0548	-6.0548	-11.055	-16.055	-21.055	-26.055	-31.055
-0.5	105.54	104.55	103.58	102.60	101.62	100.65	99.679
-0.1	89.404	88.368	87.328	86.280	85.222	84.152	81.218
0	85.956	84.951	83.944	78.967	68.967	58.967	48.967
0.1	72.684	61.573	50.462	39.351	28.240	17.129	6.0176
0.5	-266.63	-286.63	-306.63	-326.63	-346.63	-366.63	-386.63
0.99	-42268	-43268	-44268	-45268	-46268	-47268	-48268

both S_v and S_r. The singularity of R_{vc} at the point $S_r = 1$ received for this value of R_h a manifestation which is much stronger than that in the case $R_h = 20$ as seen from the values at the bottom line in Table 7.

6.5 Case for a Horizontal Thermal Rayleigh Number, $R_h = 40$

In this case, presented in Tables 9, 10, and 27 new qualitative features appear as compared to the results for $R_h \leq 30$. Specifically, all the cases with $S_r = -1$ are now non-oscillatory, the value of R_{vc} in each of these cases is negative, and oscillatory cases exist only for three values of the Soret number: $S_r = -0.5, -0.1$, and 0. Like in the cases with $R_h \leq 30$, the value of

Table 10 Values of the critical oscillatory frequency, $\omega_{rc} = \omega_r(l_c)$, for various values of S_v and S_r, for $R_h = 40$

	$S_v = -30$	-20	-10	0	10	20	30
$S_r = -1$	0	0	0	0	0	0	0
-0.5	11.073	10.688	10.259	9.8184	9.3885	8.9160	8.4251
-0.1	7.2011	6.5622	5.8314	4.9988	4.0122	2.6730	0
0	4.8461	3.7871	2.2671	0	0	0	0
0.1	0	0	0	0	0	0	0
0.5	0	0	0	0	0	0	0
0.99	0	0	0	0	0	0	0

Table 11 Values of the critical vertical thermal Rayleigh number, R_{vc}, for various values of S_v and S_r, for $R_h = 50$

	$S_v = -30$	-20	-10	0	10	20	30
$S_r = -1$	-159.31	-164.31	-169.31	-174.31	-179.31	-184.31	-189.31
-0.5	44.795	38.128	31.461	24.795	18.128	11.461	4.7950
-0.1	112.06	110.99	109.90	108.80	107.68	106.53	105.36
0	107.19	106.18	105.16	100.12	90.117	80.117	70.117
0.1	70.136	59.026	47.913	36.802	25.691	14.580	3.4690
0.5	-530.29	-550.29	-570.29	-590.29	-610.29	-630.29	-650.29
0.99	-74187	-75187	-76187	-77187	-78187	-79187	-80187

R_{vc} decays as a function with S_v, for every fixed value of S_r. Starting with $S_r = -0.5$, the value of R_{vc} decays as a function of S_r, for every fixed S_v. For each fixed value S_r except for $S_r = -0.5$ and -0.1, the value of l_c presented in Table 27 does not vary with S_v, and for each fixed S_v, it decays as a function of S_r, for $S_r \geq -0.5$.

The singular behavior of R_{vc} as $S_r \to 1^-$ is seen from the values in the two bottom lines of Table 9. The approximation given by Eq. (28) in NMG is rather poor in the cases when S_r approaches the value of 1. For instance, in the case with $S_r = 0.99$ and $S_v = 30$, in the computations we obtained the value $R_{vc} = -48268$, whereas Eq. (28) in NMG gives the value $R_{vc}^{NMG} = -39134$. Hence, the relative deviation in this case is $\delta = |R_{vc} - R_{vc}^{NMG}|/|R_{vc}| = 18.9\,\%$.

6.6 Case for a Horizontal Thermal Rayleigh Number, $R_h = 50$

The results for this case are presented in Tables 11, 12, and 28. For every fixed S_v, the value of R_{vc} as a function of S_r grows for $-1 \leq S_r \leq -0.1$ and decays for $S_r \geq -0.1$. The value of l_c does not vary with S_v, for every fixed S_r, except for $S_r = -0.1$ and 0. In the latter two cases l_c grows slightly with S_v. The set of oscillatory critical modes reduces to ten cases, for $S_r = -0.1$ and 0. In these cases, ω_{rc} is a decaying function of both S_v and S_r. Compared to the case $R_h = 40$, in the present case in the cases with $S_r = 0.99$, for each S_v, the negative value of R_{vc} is increased by the factor of about 1.7.

Table 12 Values of the critical oscillatory frequency, $\omega_{rc} = \omega_r(l_c)$, for various values of S_v and S_r, for $R_h = 50$

	$S_v = -30$	-20	-10	0	10	20	30
$S_r = -1$	0	0	0	0	0	0	0
-0.5	0	0	0	0	0	0	0
-0.1	8.3497	7.7650	7.1316	6.4456	5.6597	4.7678	3.6710
0	4.9846	3.8936	2.3231	0	0	0	0
0.1	0	0	0	0	0	0	0
0.5	0	0	0	0	0	0	0
0.99	0	0	0	0	0	0	0

Table 13 Values of the critical vertical thermal Rayleigh number, R_{vc}, for various values of S_v and S_r, for $R_h = 60$

	$S_v = -30$	-20	-10	0	10	20	30
$S_r = -1$	-395.79	-400.79	-405.79	-410.79	-415.79	-420.79	-425.79
-0.5	-76.758	-83.424	-90.091	-96.758	-103.42	-110.09	-116.76
-0.1	137.71	136.54	135.36	134.14	132.89	131.58	130.21
0	131.81	130.77	129.71	124.47	114.47	104.47	94.473
0.1	67.011	55.900	44.789	33.678	22.567	11.456	0.34479
0.5	-871.78	-891.78	-911.78	-931.78	-951.78	-971.78	-991.78
0.99	-114362	-115362	-116362	-117362	-118362	-119362	-120362

Table 14 Values of the critical oscillatory frequency, $\omega_{rc} = \omega_r(l_c)$, for various values of S_v and S_r, for $R_h = 60$

	$S_v = -30$	-20	-10	0	10	20	30
$S_r = -1$	0	0	0	0	0	0	0
-0.5	0	0	0	0	0	0	0
-0.1	9.4792	8.8741	8.2421	7.5493	6.7966	5.9487	4.956
0	5.3115	4.1339	2.4398	0	0	0	0
0.1	0	0	0	0	0	0	0
0.5	0	0	0	0	0	0	0
0.99	0	0	0	0	0	0	0

6.7 Case for a Horizontal Thermal Rayleigh Number, $R_h = 60$

The results for this case presented in Tables 13, 14, and 29 are qualitatively similar to the results for the case $R_h = 50$. For each fixed S_v, The critical vertical thermal Rayleigh number, R_{vc}, attains its maximum, for $S_r = -0.1$, and, as $S_r \to 0.99$, it decays sharply to large negative values of the order of 1.1×10^5. There are ten cases of critical oscillatory modes, for the same pairs (S_v, S_r) like in case $R_h = 50$, for each fixed value of S_r, except for $S_r = -0.1$ and 0, the value of l_c does not vary with S_v and for the two latter values it increases slightly with S_v.

Table 15 Values of the group velocity of the wavepacket, $V_g = d\omega_r(l_r)/dl_r$ at $l_r = l_c$, for the marginally supercritical value of the vertical Rayleigh number R_{vc}, for various values of S_v and S_r, for $R_h = 0$

	$S_v = -30$	-20	-10	0	10	20	30
$S_r = -1$	0	0	0	0	0	0	0
-0.5	0	0	0	0	0	0	0
-0.1	1.3562	0.97433	0.24356	0	0	0	0
0	1.5177	1.1854	0.71123	0	0	0	0
0.1	1.6637	1.3630	0.97357	0.19456	0	0	0
0.5	2.1506	1.9170	1.6507	1.3322	0.90823	0	0
1	2.6356	2.4385	2.2240	1.9865	1.7165	1.3951	0.97273

Table 16 Values of the group velocity of the wavepacket, $V_g = d\omega_r(l_r)/dl_r$ at $l_r = l_c$, for the marginally supercritical value of the vertical Rayleigh number R_{vc}, for various values of S_v and S_r, for $R_h = 10$

	$S_v = -30$	-20	-10	0	10	20	30
$S_r = -1$	0	0	0	0	0	0	0
-0.5	1.0074	0.40621	0	0	0	0	0
-0.1	1.4346	1.0808	0.52776	0	0	0	0
0	1.5167	1.1854	0.71082	0	0	0	0
0.1	1.5925	1.2751	0.84578	0	0	0	0
0.5	1.8469	1.5679	1.2269	0.74227	0	0	0
1	2.0877	1.8281	1.5277	1.1505	0.55886	0	0

Table 17 Values of the group velocity of the wavepacket, $V_g = d\omega_r(l_r)/dl_r$ at $l_r = l_c$, for the marginally supercritical value of the vertical Rayleigh number R_{vc}, for various values of S_v and S_r, for $R_h = 20$

	$S_v = -30$	-20	-10	0	10	20	30
$S_r = -1$	1.8931	1.6550	1.3766	1.0367	0.58236	0.17669	0
-0.5	1.9001	1.6621	1.3782	1.0249	0.49002	0	0
-0.1	1.6369	1.3389	0.95249	0.16714	0	0	0
0	1.5186	1.1843	0.70943	0	0	0	0
0.1	1.3641	0.97190	0.16223	0	0	0	0
0.5	0	0	0	0	0	0	0
0.99	0	0	0	0	0	0	0

7 Absolute/Convective Instability Dichotomy

The results for the absolute/convective instability dichotomy, for the cases treated in Sect. 21, are presented in this section in Tables 15, 16, 17, 18, 19, 20, 21. A comparison of the results for the group velocity, V_g, of the emerging marginally unstable wavepacket in these tables with the results for the critical oscillatory frequency, ω_{rc}, for the corresponding cases presented in Tables 2, 4, 6, 8, 10, 12, and 14, for the cases $R_h = 0$, 10, 20, 30, 40, 50, and 60, respectively, shows that at the onset of convection the destabilization is through absolute instability if and only if the critical modes are non-oscillatory. In the cases when the destabilization is through

Table 18 Values of the group velocity of the wavepacket, $V_g = d\omega_r(l_r)/dl_r$ at $l_r = l_c$, for the marginally supercritical value of the vertical Rayleigh number R_{vc}, for various values of S_v and S_r, for $R_h = 30$

	$S_v = -30$	-20	-10	0	10	20	30
$S_r = -1$	2.4853	2.3080	2.1187	1.9144	1.6895	1.4419	1.1636
-0.5	2.5039	2.3242	2.1295	1.9172	1.6796	1.4084	1.0871
-0.1	1.8748	1.6244	1.3292	0.95497	0.28180	0	0
0	1.5145	1.1798	0.70440	0	0	0	0
0.1	0.8541	0	0	0	0	0	0
0.5	0	0	0	0	0	0	0
0.99	0	0	0	0	0	0	0

Table 19 Values of the group velocity of the wavepacket, $V_g = d\omega_r(l_r)/dl_r$ at $l_r = l_c$, for the marginally supercritical value of the vertical Rayleigh number R_{vc}, for various values of S_v and S_r, for $R_h = 40$

	$S_v = -30$	-20	-10	0	10	20	30
$S_r = -1$	0	0	0	0	0	0	0
-0.5	2.5541	2.3833	2.2065	2.0178	1.8080	1.5870	1.3447
-0.1	2.0482	1.8322	1.5854	1.2984	0.94790	0.41782	0
0	1.4975	1.1668	0.68781	0	0	0	0
0.1	0	0	0	0	0	0	0
0.5	0	0	0	0	0	0	0
0.99	0	0	0	0	0	0	0

Table 20 Values of the group velocity of the wavepacket, $V_g = d\omega_r(l_r)/dl_r$ at $l_r = l_c$, for the marginally supercritical value of the vertical Rayleigh number R_{vc}, for various values of S_v and S_r, for $R_h = 50$

	$S_v = -30$	-20	-10	0	10	20	30
$S_r = -1$	0	0	0	0	0	0	0
-0.5	0	0	0	0	0	0	0
-0.1	2.0225	1.8137	1.5845	1.3283	1.0316	0.67078	0.17474
0	1.4671	1.1336	0.6474	0	0	0	0
0.1	0	0	0	0	0	0	0
0.5	0	0	0	0	0	0	0
0.99	0	0	0	0	0	0	0

convective instability, for $R_h = 0$ and 10, the group velocity, V_g, is a decaying function of S_v and growing function of S_r. In all the cases with $R_h \geq 20$, except for the interval $R_h = 60$, $S_r = -0.1, 20 < S_v < 30$, the group velocity is a decaying function of both S_v and S_r. For $R_h \geq 40$, the base state is absolutely unstable at the onset of convection, for all $S_r \geq 0.1$ considered. As R_h increases starting with $R_h = 30$, the number of the parameter cases in which the base state is absolutely unstable increases from 26, for $R_h = 30$, to 39, for $R_h = 60$. For $R_h \geq 50$, only for two values of the Soret number, $S_r = -0.1$ and 0, there exist parameter combinations for which the marginally unstable base state is absolutely stable, but convectively unstable. In the cases $R_h = 50$ and $R_h = 60$, the sets of the convectively unstable, but absolutely stable cases are the same, whereas the group velocity in all such

Table 21 Values of the group velocity of the wavepacket, $V_g = d\omega_r(l_r)/dl_r$ at $l_r = l_c$, for the marginally supercritical value of the vertical Rayleigh number R_{vc}, for various values of S_v and S_r, for $R_h = 60$

	$S_v = -30$	-20	-10	0	10	20	30
$S_r = -1$	0	0	0	0	0	0	0
-0.5	0	0	0	0	0	0	0
-0.1	1.4946	1.2600	0.99643	0.70500	0.36268	0.05281	0.59940
0	1.3971	1.0547	0.54487	0	0	0	0
0.1	0	0	0	0	0	0	0
0.5	0	0	0	0	0	0	0
0.99	0	0	0	0	0	0	0

Table 22 Maximum value of the group velocity of the wavepacket, V_g, for the marginally supercritical value of the vertical Rayleigh number, R_{vc}, for various values of R_h. The maximum in each case is attained for $S_v = -30$ at the value of S_r indicated

	$R_h = 0$	10	20	30	40	50	60
V_g	2.6356	2.0877	1.8931	2.4853	2.5541	2.0225	1.4946
S_r	1	1	-1	-1	-0.5	-0.1	-0.1

cases, except for the case with $S_v = 30$, is smaller for the cases with $R_h = 60$ than for those with $R_h = 50$.

The maximum group velocity, for each fixed values of R_h, is attained for $S_v = -30$. In Table 22, the values of the maximum group velocity, for various values of R_h, are shown for the values of S_r at which the maximum is attained.

8 Conclusions

In this article, we analyzed how the Soret effect influences the nature of the destabilization of a flow in a saturated horizontal extended porous layer with vertical solutal and inclined thermal gradients.

As in the previous studies of similar models of flow in porous media, but without the Soret effect (see Brevdo 2009, Brevdo and Ruderman 2009a,b, Diaz and Brevdo 2011, 2012), we found that in the model treated the absolute/convective instability dichotomy exists as well, and that these two types of instability are present for non-vanishing values of the Soret number depending on the values of the other control parameters. As the horizontal thermal Rayleigh number, R_h, increases from $R_h = 30$ to $R_h = 60$, the number of cases at which the base state is absolutely stable, but convectively unstable decreases from 21 to 10. The maximum value of the group velocity of the wavepacket for the marginally supercritical base state is attained for $S_v = -30$ and all the values of R_h considered at non-zero values of the Soret number. In this study, we have not addressed the question of whether at the point of destabilization the marginally unstable base state is genuinely convectively unstable, but absolutely stable. This question can be addressed by evaluating the value of vertical thermal Rayleigh number, R_{vt}, at which the transition from convective to absolute instability occurs

and computing its relative deviation from the critical vertical thermal Rayleigh number, R_{vc}, as it was done in Diaz and Brevdo (2012). A treatment of this question is left as a future task.

The findings in the article, together with the findings in the papers cited above, indicate that the absolute/convective instability dichotomy is a characteristic feature of flows in porous media. The dichotomy can hopefully be used for investigating numerically and in experiments one of the open question of the theory of turbulent transition. Specifically: does a fully developed nonlinear regime that emerges in a linearly absolutely unstable base flow possess essentially different qualitative features from those of a fully developed nonlinear state that evolves in an absolutely stable, but convectively unstable flow?

Acknowledgments This study was partially supported by a Research Grant of the DAAD (German Academic Exchange Service). Part of the research was carried out during a three-month visit of Prof. L. Brevdo at the Department of Geosciences of the University of Tübingen. The hospitality of the Department is acknowledged with gratitude. L. B. acknowledges constant encouragement and interest of Elisabeth Juchem-Brevdo.

Appendix: Values of the Critical Wavenumber, l_c

See Tables 23, 24, 25, 26, 27, 28, 29.

Table 23 Values of the critical wavenumber, l_c, for various values of S_v and S_r, for $R_h = 0$

	$S_v = -30$	-20	-10	0	10	20	30
$S_r = -1$	3.136	3.136	3.141	3.144	3.144	3.144	3.144
$S_r = -0.5, -0.1, 0, 0.1, 0.5, 1$	3.141	3.141	3.141	3.141	3.141	3.141	3.141

Table 24 Values of the critical wavenumber, l_c, for various values of S_v and S_r, for $R_h = 10$

	$S_v = -30$	-20	-10	0	10	20	30
$S_r = -1$	3.180	3.180	3.180	3.180	3.180	3.180	3.180
-0.5	3.140	3.140	3.152	3.152	3.152	3.152	3.152
-0.1	3.140	3.140	3.140	3.144	3.144	3.144	3.144
0	3.140	3.140	3.140	3.140	3.140	3.140	3.140
0.1	3.140	3.140	3.140	3.140	3.140	3.140	3.140
0.5	3.140	3.140	3.140	3.140	3.140	3.140	3.148
1	3.140	3.136	3.136	3.136	3.136	3.164	3.164

Table 25 Values of the critical wavenumber, l_c, for various values of S_v and S_r, for $R_h = 20$

	$S_v = -30$	-20	-10	0	10	20	30
$S_r = -1$	3.100	3.096	3.088	3.080	3.072	3.064	4.560
-0.5	3.136	3.140	3.136	3.136	3.136	3.363	3.360
-0.1	3.147	3.147	3.147	3.147	3.160	3.160	3.160
0	3.147	3.147	3.147	3.147	3.147	3.147	3.147
0.1	3.141	3.141	3.141	3.141	3.141	3.141	3.141
0.5	3.221	3.221	3.221	3.221	3.221	3.221	3.221
0.99	3.520	3.520	3.520	3.520	3.520	3.520	3.520

Table 26 Values of the critical wavenumber, l_c, for various values of S_v and S_r, for $R_h = 30$

	$S_v = -30$	-20	-10	0	10	20	30
$S_r = -1$	3.000	2.993	2.980	2.964	2.952	2.936	2.920
-0.5	3.132	3.129	3.125	3.125	3.120	3.115	3.106
-0.1	3.167	3.167	3.167	3.171	3.171	3.246	3.246
0	3.162	3.162	3.162	3.162	3.162	3.162	3.162
0.1	3.143	3.143	3.143	3.143	3.143	3.143	3.143
0.5	3.536	3.536	3.536	3.536	3.536	3.536	3.536
0.99	4.673	4.673	4.673	4.673	4.673	4.673	4.673

Table 27 Values of the critical wavenumber, l_c, for various values of S_v and S_r, for $R_h = 40$

	$S_v = -30$	-20	-10	0	10	20	30
$S_r = -1$	11.26	11.26	11.26	11.26	11.26	11.26	11.26
-0.5	3.120	3.120	3.107	3.093	3.093	3.080	3.067
-0.1	3.220	3.230	3.230	3.230	3.240	3.240	3.580
0	3.200	3.210	3.220	3.220	3.220	3.220	3.220
0.1	3.140	3.140	3.140	3.140	3.140	3.140	3.140
0.5	4.283	4.283	4.283	4.283	4.283	4.283	4.283
0.99	5.667	5.667	5.667	5.667	5.667	5.667	5.667

Table 28 Values of the critical wavenumber, l_c, for various values of S_v and S_r, for $R_h = 50$

	$S_v = -30$	-20	-10	0	10	20	30
$S_r = -1$	13.40	13.40	13.40	13.40	13.40	13.40	13.40
-0.5	10.52	10.52	10.52	10.52	10.52	10.52	10.52
-0.1	3.360	3.367	3.373	3.387	3.387	3.400	3.427
0	3.307	3.307	3.320	3.342	3.343	3.343	3.343
0.1	3.147	3.147	3.147	3.147	3.147	3.147	3.147
0.5	5.093	5.093	5.093	5.093	5.093	5.093	5.093
0.99	6.373	6.373	6.373	6.373	6.373	6.373	6.373

Table 29 Values of the critical wavenumber, l_c, for various values of S_v and S_r, for $R_h = 60$

	$S_v = -30$	-20	-10	0	10	20	30
$S_r = -1$	15.36	15.36	15.36	15.36	15.36	15.36	15.36
-0.5	12.17	12.17	12.17	12.17	12.17	12.17	12.17
-0.1	3.713	3.720	3.740	3.753	3.780	3.813	3.853
0	3.567	3.573	3.580	3.673	3.673	3.673	3.673
0.1	3.147	3.147	3.147	3.147	3.147	3.147	3.147
0.5	5.707	5.707	5.707	5.707	5.707	5.707	5.707
0.99	6.960	6.960	6.960	6.960	6.960	6.960	6.960

References

Bahloul, A., Boutana, N., Vasseur, P.: Double-diffusive and Soret-induced convection in a shallow horizontal porous layer. J. Fluid Mech. **491**, 325–352 (2003)

Bear, J.: Dynamics of Fluids in Porous Media. Dover Publications, New York (1972)

Bers, A.: Theory of absolute and convective instabilities. In: Auer, G., Cap, F. (eds.) Survey Lectures. Proc. Int. Congr. Waves and instabilities in plasmas, pp. B1–B52. Institute for Theoretical Physics, Innsbruck, Austria (1973)

Brevdo, L.: Three-dimensional absolute and convective instabilities, and spatially amplifying waves in parallel shear flows. Z. Angew. Math. Phys. **42**, 911–942 (1991)

Brevdo, L.: A dynamical system approach to the absolute instability of spatially developing localized open flows and media. Proc. R. Soc. Lond. A **458**, 1375–1397 (2002)

Brevdo, L.: Global and absolute instabilities of spatially developing open flows and media with algebraically decaying tails. Proc. R. Soc. Lond. A **459**, 1403–1425 (2003)

Brevdo, L.: Linear stability theory for fronts with algebraically decaying tails. Proc. R. Soc. Lond. A **460**, 3013–3035 (2004)

Brevdo, L.: Convectively unstable wave packets in spatially developing open flows and media with algebraically decaying tails. Proc. R. Soc. Lond. A **461**, 1–20 (2005)

Brevdo, L.: Three-dimensional absolute and convective instabilities at the onset of convection in a porous medium with inclined temperature gradient and vertical throughflow. J. Fluid Mech. **641**, 475–487 (2009)

Brevdo, L., Bridges, T.J.: Absolute and convective instabilities of spatially periodic flows. Phil. Trans. R. Soc. Lond. A **354**, 1027–1064 (1996)

Brevdo, L., Ruderman, M.S.: On the convection in a porous medium with inclined temperature gradient and vertical throughflow. Part I. Normal modes. Transp. Porous Media **80**, 137–151 (2009a)

Brevdo, L., Ruderman, M.S.: On the convection in a porous medium with inclined temperature gradient and vertical throughflow. Part II. Absolute and convective instabilities, and spatially amplifying waves. Transp. Porous Media **80**, 153–172 (2009b)

Briggs, R.J.: Electron–Stream Interaction with Plasmas. MIT Press, Cambridge, MA (1964)

Diaz, E., Brevdo, L.: Absolute/convective instability dichotomy at the onset of convection in a porous layer with either horizontal or vertical solutal and inclined thermal gradients, and horizontal throughflow. J. Fluid Mech. **681**, 567–596 (2011)

Diaz, E., Brevdo, L.: Transition from convective to absolute instability in a porous layer with either horizontal or vertical solutal and inclined thermal gradients, and horizontal throughflow. Transp. Porous Media **92**, 597–617 (2012)

Drazin, P.G., Reid, W.H.: Hydrodynamic Stability. Cambridge University Press, Cambridge (1989)

Guo, J., Kaloni, P.N.: Nonlinear stability and convection induced by inclined thermal and solutal gradients. Z. Angew. Math. Phys. **46**, 645–654 (1995)

Ludwig, C.: Diffusion zwischen ungleich erwärmten Orten gleich zusammengesetzter Lösungen. Sitz. Kais. Akad. Wiss. (Math.-Naturwiss. Cl.), Wien **65**, 539 (1856)

Manole, D.M., Lage, J.L., Nield, D.A.: Convection induced by inclined thermal and solutal gradients, with horizontal mass flow, in a shallow horizontal layer of a porous medium. Int. J. Heat Mass Transf. **37**, 2047–2057 (1994)

Marcoux, M., Charrier-Mojtabi, M.-C.: Etude paramétrique de la thermogravitation en milieu poreux. C.R. Acad. Sci. Paris (II B) **326**, 539–546 (1998)

Narayana, P.A.L., Murthy, P.V.S.N., Gorla, R.S.R.: Soret-driven thermo solutal convection induced by inclined thermal and solutal gradients in a shallow horizontal layer of a porous medium. J. Fluid Mech. **612**, 1–19 (2008)

Nield, D.A.: Convection in a porous medium with inclined temperature gradient. Int. J. Heat Mass Transf. **34**, 87–92 (1991)

Nield, D.A.: Convection in a porous medium with inclined temperature gradient: additional results. Int. J. Heat Mass Transf. **37**, 3021–3025 (1994)

Nield, D.A.: Convection in a porous medium with inclined temperature gradient and vertical throughflow. Int. J. Heat Mass Transf. **41**, 241–243 (1998)

Nield, D.A., Bejan, A.: Convection in Porous Media. Springer, Berlin (2006)

Nield, D.A., Manole, D.M., Lage, J.L.: Convection induced by inclined thermal and solutal gradients in a shallow horizontal layer of a porous medium. J. Fluid Mech. **257**, 559–574 (1993)

Platten, J.K.: The Soret effect: a review of recent experimental results. J. Appl. Mech. **73**, 5–15 (2006)

Platten, J.K., Bou-Ali, M.M., Blanco, P., Madariaga, J.A., Santamaria, C.: Soret coefficients in some water–methanol, water–ethanol, and water–isopropanol Systems. J. Phys. Chem. B **111**, 11524–11530 (2007)

Qiao, Z., Kaloni, P.N.: Convection induced by inclined temperature gradient with mass flow in a porous medium. Trans. ASME J. Heat Transf. **119**, 366–370 (1997)

Qiao, Z., Kaloni, P.N.: Non-linear convection in a porous medium with inclined temperature. Int. J. Heat Mass Transf. **41**, 2549–2552 (1998)

Sarkar, A., Phillips, O.M.: Effects of horizontal gradients on thermohaline instabilities in a thick porous layer. Phys. Fluids A **4**, 1165–1175 (1992)

Soret, Ch.: Sur l'état d'équilibre que prend au point de vue de sa concentration une dissolution saline primitivement homohéne dont deux parties sont portées à des températures différentes. Arch. Sci. Phys. Nat. **2**, 48–61 (1879)

Sovran, O., Charrier-Mojtabi, M.-C., Mojtabi, A.: Naissance de la convection thermo-solutale en couche poreuse infinie avec effet Soret. C.R. Acad. Sci. Paris (II B) **329**, 287–293 (2001)

Straughan, B.: The Energy Method, Stability and Nonlinear Convection, 2nd ed. Springer, Berlin (2004)

Straughan, B., Walker, D.W.: Two very accurate and efficient methods for computing eigenvalues and eigenfunctions in porous convection problems. J. Comput. Phys. **127**, 128–141 (1996)

Weber, J.E.: Convection in a porous medium with horizontal and vertical temperature gradients. Int. J. Heat Mass Transf. **17**, 241–248 (1974)